Journal of Catalysis 274 (2010) 64–75

Contents lists available at ScienceDirect

Journal of Catalysis

journal homepage: www.elsevier.com/locate/jcat

Structure of flame-made vanadia/silica and catalytic behavior in the oxidative dehydrogenation of propane

Bjoern Schimmoeller [a], Yijiao Jiang [b], Sotiris E. Pratsinis [a], Alfons Baiker [b,*]

[a] Particle Technology Laboratory, Department of Mechanical and Process Engineering, ETH Zurich, CH-8092 Zurich, Switzerland
[b] Institute for Chemical and Bioengineering, Department of Chemistry and Applied Biosciences, ETH Zurich, Hönggerberg, HCI, CH-8093 Zurich, Switzerland

ARTICLE INFO

Article history:
Received 9 April 2010
Revised 28 May 2010
Accepted 3 June 2010
Available online 14 July 2010

Keywords:
Flame spray pyrolysis
Raman spectroscopy
^{51}V MAS NMR
V surface density
V_2O_5/SiO_2
Oxidative dehydrogenation of propane

ABSTRACT

Vanadia/silica particles with a specific surface area up to 330 $m^2\ g^{-1}$ and a V_2O_5 content up to 50 wt.% or V surface density up to 27.6 V nm^{-2} were prepared by flame spray pyrolysis. The catalysts were characterized by nitrogen adsorption, X-ray diffraction, temperature-programmed reduction, Raman spectroscopy, and ^{51}V MAS NMR and tested in the oxidative dehydrogenation (ODH) of propane. Depending on vanadia content, different vanadia species were formed. The as-prepared flame-made catalysts showed dominantly isolated monomeric VO_x surface species for V loadings exceeding even the typical "monolayer coverage" (2 V nm^{-2}) of classic wet-impregnated materials. The stability of these VO_x species depended on temperature and V surface density. Catalysts with 3.3 V nm^{-2} were stable up to 500 °C and those with 2 V nm^{-2} up to 600 °C. Catalysts loaded with 3–25 wt.% V_2O_5 were tested for the ODH of propane. Catalysts containing $\geqslant$15 wt.% V_2O_5 showed structural rearrangement of the VO_x species during the catalytic tests inducing a transition from monomeric to crystalline vanadia. The turnover frequency of flame-made catalysts decreased with increasing vanadia loading, indicating a higher activity of monomeric VO_x species compared to crystalline V_2O_5. The conversion (global activity), however, showed a maximum for the 20 wt.% V_2O_5/SiO_2 (4.6 V nm^{-2}) catalyst. The selectivity to propene depended mainly on propane conversion and only to a lesser extent on the structure of the VO_x species. Highest selectivity (55%) was achieved for the low loaded catalysts. With increasing vanadia loading, formation of CO_x increased and the product ratio of CO_2/CO decreased. Highest propene yield was measured for catalysts with relative high V surface density containing both monomeric VO_x and crystalline V_2O_5. Flame spray pyrolysis proved to be a very versatile method for synthesis of V_2O_5/SiO_2 catalysts with high dispersion of isolated VO_x species at high surface density.

1. Introduction

Propene is one of the most important feedstock in the chemical industry as it is used for the synthesis of various chemical intermediates and major processes such as polypropene (PP) synthesis. Polypropene is used for the production of diverse products, ranging from solvents to plastics. At the present time, steam cracking, fluid-catalytic-cracking, and catalytic dehydrogenations are the main processes to gain olefins from natural feedstock oil [1]. Increasing oil prices and growing PP market (4–5% per year) spur the development of a less energy-intensive process for the propene production [2]. One of the promising processes is the oxidative dehydrogenation (ODH) of propane to propene. This process will allow to use propane of natural gas stocks, in a range of 2–5% [3], as a feedstock for the propene/PP production.

Catalyst based on supported vanadia showed promising results for the ODH reaction. It is commonly agreed that vanadium oxide can be present on the support oxide in three distinct forms: i.e. as monomeric VO_x species at low loadings (typical <2.3 V nm^{-2}), as oligomeric form at medium loadings (2.3–7.5 V nm^{-2}), and as V_2O_5 crystals at high loadings (>8 V nm^{-2}) [4–7]. The composition of VO_x species and thus the catalytic behavior of supported vanadia catalysts are influenced by the specific surface area (SSA), V_2O_5 content, the composition of the support [6,8–10], and also by the synthesis method [11–13]. For SiO_2-supported catalysts, the transition from amorphous monomeric to crystalline vanadia occurs already at low V surface densities around 2 V nm^{-2} [10] or even lower [2,14], without exhibiting any oligomeric VO_x species in the transition range.

The activity of vanadia species in the ODH reaction can depend significantly on the supporting oxide [6,10]. The role of the structure of the VO_x species on the support surface on activity and selectivity is still debated and not completely resolved. Khodakov et al. [6] stated that oligomeric VO_x species or even small V_2O_5 crystallites are more active and selective than isolated monomeric sites independent of the supporting oxide (TiO_2, SiO_2, Al_2O_3, ZrO_2, and HfO_2). Tian et al. [10] stated that the relative rate of propene

* Corresponding author. Fax: +41 44 632 1163.
E-mail address: baiker@chem.ethz.ch (A. Baiker).

0021-9517/$ - see front matter © 2010 Elsevier Inc. All rights reserved.
doi:10.1016/j.jcat.2010.06.005

formation does not depend on the nature of the support (SiO_2, Al_2O_3, and ZrO_2), or V surface density and structure (mono- and oligomeric), in agreement with previous studies [15]. For silica-supported vanadia-based catalysts, however, several authors reported turn-over-frequencies that differ up to one order of magnitude depending on V surface density. Monomeric VO_x species were identified as the most active and selective V sites in the ODH of propane [2,14,16–18].

Most of these catalysts were prepared using classic, multiple-step, wet-phase processes (e.g. impregnation) of the corresponding non- or mesoporous support. Good accessibility of the VO_x species is important for high activity and selectivity. The dispersion and structure of the VO_x species and thus their catalytic performance depend not only on the composition of the supporting oxide but also on the catalyst synthesis method, like vapor-fed flame synthesis [19], flame spray pyrolysis [11,13], sputter deposition [20], or atomic layer deposition [12]. Especially the wet-chemistry synthesis routes sometimes show broad variation in the structure of the VO_x species depending on the synthesis conditions.

A highly reproducible synthesis method leading to easy accessible model catalysts of high purity is flame spray pyrolysis (FSP), a one-step process suitable for producing mixed metal-oxide catalysts with excellent control of particle morphology and reproducibility [13,21–23]. In the FSP process, the VO_x is formed on the oxide support surface due to the lower melting point (~700 °C) of V_2O_5 compared to the oxide supports (melting point usually >1000 °C). The vanadia layer is formed when the flame temperature is low enough for it to condense out in vapor-fed [13,19] and liquid-fed flame synthesis [13]. With this process, catalysts with significant differences in particle structure and VO_x species composition can be produced. FSP-made V_2O_5/TiO_2 catalysts exhibit monomeric and oligomeric VO_x species at high V surface densities where the corresponding wet-made catalysts form crystalline VO_x species [13]. Recently, V_2O_5/SiO_2 catalysts were prepared by flame pyrolysis [11] that showed a relative low surface area (<80 $m^2\,g^{-1}$) for flame-made silica-supported materials [24,25] and a high V dispersion in the bulk of the particles which can probably be traced to their use of low enthalpy solvents and low dispersion of the liquid precursor that may have resulted in catalysts by droplet-to-particle formation rather than nucleation from the gas phase [23]. Only 30% of the nominal V atoms were accessible for the reaction. Particularly, the low vanadia content catalysts showed almost no selectivity to propene [11]. The aim of the present work was to explore the potential of flame spray pyrolysis for synthesis of non-porous, nanostructured V_2O_5/SiO_2 catalysts for the oxidative dehydrogenation of propane (ODH). A focal point was the effect of FSP synthesis on the structural properties of V_2O_5/SiO_2 catalysts and catalytic performance. For this purpose, catalysts with different V loadings were prepared, characterized with various physicochemical techniques, and tested in ODH.

2. Experimental

2.1. Catalyst preparation

Nanostructured vanadia/silica particles were made by FSP of appropriate precursor solutions [13,26]. For the vanadium precursor, ammonium metavanadate (Sigma–Aldrich, 99%) was mixed with 2-ethylhexanoic acid (2-EHA, Riedel-de Haën, >99%) and acetic anhydride (Riedel-de Haën, >99%) in a ratio of 2:1 under stirring and heating it to 100 °C for several hours resulting in a metal concentration of 0.5 M. Then, appropriate amounts of hexamethyldisiloxane (Aldrich, >98%) and the vanadium precursor were mixed based on the nominal weight content vanadia in the catalyst (0–50 wt.%) with xylene (Riedel-de Haën, >96%) and 2-EHA (Riedel-de Haën, >99%) in a ratio of 1:1 resulting in a total metal concentration of 0.75 mol L^{-1}. The use of solvents (xylene, 2-EHA) with significantly higher combustion enthalpy (≈4600 kJ mol^{-1}) ensured high enthalpy density in the flame and particle formation via nucleation from the gas phase [27,28]. Moreover, the O_2 pressure drop was adjusted to 1.7 bar for high dispersion of the liquid precursor spray and the flow rates (enthalpy) of the pilot flame were tripled (CH_4: 1.5 L min^{-1}, O_2: 3.3 L min^{-1}) compared to Rossetti et al. [11]. Solubility and stability of the metal precursors were no problem for the whole investigated range of vanadia contents.

This precursor solution was fed by a syringe pump (Inotec, IER-560) through the FSP nozzle and dispersed by O_2 (PanGas, 99.95%, 5 L min^{-1}) into a fine spray that was ignited and sustained by a premixed CH_4/O_2 flame. Additional 5 L min^{-1} of sheath O_2 was fed in the reactor to ensure complete combustion. A detailed description of the laboratory scale FSP reactor can be found elsewhere [26]. The powders were collected with the aid of a vacuum pump (Busch SV 1050 B) on a glass microfiber filter (Whatman GF/D, 257 mm in diamater).

2.2. Catalyst characterization

The specific surface area (SSA, $m^2\,g^{-1}$) of the powder was determined by nitrogen adsorption (Pan Gas, >99.999%) at 77 K using the Brunauer–Emmett–Teller (BET) method (Micromeritics Tristar 3000) with a five point-isotherm ($0.05 < p/p_0 < 0.25$). Accounting for the V_2O_5 content in the powder density, the average particle size (d_{BET}) was calculated assuming spherical particles. Full BET adsorption–desorption isotherms were measured on the same instrument. X-ray diffraction (XRD) was measured on a Bruker D8 Advance diffractometer (step size of 0.03°, scan speed of 0.60° min^{-1}, Cu Kα radiation).

Temperature-programmed reduction (TPR) was used for determination of the average oxidation state (AOS) after reduction and reducibility of vanadia. Experiments were carried out on a Micromeritics Autochem II 2920 equipped with a TCD-detector by flowing 5 vol.% H_2 in Ar (Pan Gas, >99.999%, 10 mL min^{-1}) through the sample. The temperature was increased from 50 to 950 °C at 10 °C min^{-1}. Prior to this analysis, the sample was oxidized in flowing oxygen (PanGas, >99.999%, 20 mL min^{-1}) at 500 °C for 30 min to assure complete oxidation of vanadium species.

Raman spectroscopy was performed (Renishaw InVia Reflex Raman) with a 514-nm diode (Ar-ion laser, 25 mW) laser as excitation source focused with a microscope (Leica, magnification 50×). For the dehydrated Raman analysis, an *in-situ* cell equipped with a quartz window was used [13]. The samples were pressed into tablets and placed in the cell and then directly heated up to 500 °C under flowing synthetic air (PanGas, 99.999%, 40 mL min^{-1}). The spectra were recorded at 500 °C for 40 s and 20 accumulations to obtain sufficient signal-to-noise ratio and collected on a CCD camera after being diffracted by a prism (1800 lines per millimeter) using 12.5-mW laser energy.

The ^{51}V MAS NMR experiments were performed at room temperature on a Bruker MSL-400 spectrometer at a resonance frequency of 105.25 MHz using a 4-mm MAS NMR probe. NMR measurements were taken on as-prepared (hydrated) and on dehydrated samples. In the latter case, the catalysts were treated in a furnace at 500 °C (10 K min^{-1}) for 2 h under vacuum, subsequently transferred without any contact to air into a glove box purged with dry N_2 and filled into the 4-mm MAS rotor. In the experiments, a single pulse length of $\pi/8$ and a relaxation delay of 0.5 s, and a spinning rate of ca. 12.5 kHz were used. The ^{51}V chemical shift was referenced to vanadium trichloride oxide ($VOCl_3$). The NMR data were processed with the Bruker software WINNMR. Anisotropic shift values were obtained from the simulated MAS NMR spectra with the Bruker WINFIT software.

Table 1
Chemical and textural properties of flame-made V_2O_5/SiO_2 catalysts: composition, BET surface area (SSA), V surface density, temperature of maximal reduction rate (TPR T_{max}), and average oxidation state (AOS).

Sample	V_2O_5 content (wt.%)	SSA ($m^2\ g^{-1}$)	VO_x-density (#V nm^{-2})	TPR T_{max} (°C)	AOS
0V—Si	0	292	–	–	–
3V—Si	3	333	0.6	587	3.8
5V—Si	5	331	1.0	594	3.8
10V—Si	10	333	2.0	592	3.6
15V—Si	15	300	3.3	587	3.5
20V—Si	20	284	4.6	596	3.6
25V—Si	25	238	6.9	609	3.5
30V—Si	30	208	11.4	605	3.5
40V—Si	40	168	15.6	618	3.5
50V—Si	50	119	27.6	623	3.6

For transmission electron microscopy (TEM), the material was dispersed in ethanol and deposited onto a perforated carbon foil supported on a copper grid. The investigations were made on a Tecnai F30 microscope (field emission cathode, operated at 300 kV).

Samples are designated as xV—Si, where x denotes the V_2O_5 content in wt.% (Table 1). An as-prepared catalyst (3V—Si) was subjected to an additional heat treatment between 400 and 600 °C for 5 h (5 °C min^{-1} heating rate) in air in an oven (Carbolite, CWF 1300).

2.3. Catalytic tests

Oxidative dehydrogenation of propane was performed on a laboratory-scale test plant (Celpat GmbH) in an isothermal, plug-flow fixed-bed reactor (i.d. 15 mm). All gases (N_2, >99.996%, O_2, >99.95%, and C_3H_8, >99.5%) were fed by mass-flow controllers (Brooks). The temperature was varied in the range of 400–550 °C at atmospheric pressure. The molar fractions of propane and oxygen in the reactor feed were 0.2. Total gas flows ranged from 125 to 200 mL min^{-1} at standard conditions, resulting in a gas hourly space velocity (GHSV) in the range of 37,500–60,000 L kg_{cat}^{-1} h^{-1}. Analysis of all organic species was performed on-line by GC (Agilent, HP-PLOT-Q column, 30 m long, 0.32 mm in diameter and 0.2 μm thick) using CH_4 as internal standard while CO/CO_2 were measured by non-dispersive IR spectroscopy (ABB, Ureas). While the overall carbon balance (educts vs. products) was greater than 98%, the carbon balance of only the converted propane was closed to 92 ± 5% by summation of the products (C_3H_6, C_3H_4O, C_2H_4, C_2H_4O, CO, and CO_2). TGA analysis of the spent catalysts showed no significant loss due to carbon burn off, while Raman showed trace amounts of carbon indicated by a band around 1600 cm^{-1} for some catalysts which could be responsible for the variation in the carbon balance.

For the catalytic tests the flame-made V_2O_5/SiO_2 catalysts were pressed (2t), crushed, and fractioned (315–450 μm). Two hundred milligrams of catalyst was diluted with 20 g of SiC (<300 μm) resulting in a catalyst bed length of 60 mm to ensure good temperature control in the catalytic bed during the experiments. Reaction temperature was measured 10 mm after beginning of the catalyst bed by means of a thermocouple in the axial center of the reactor. Each catalyst was heated to 500 °C in flowing N_2/O_2 (150 ml min^{-1}, 4:1 by volume), kept there for 1 h, and then cooled down to 400 °C prior to the catalytic measurements.

3. Results and discussion

3.1. Catalyst preparation and structural properties

A pronounced color change of the synthesized powders was observed when removing the powder collection filter from the setup. Being almost completely white on the still warm filter for low V_2O_5 contents (<10 wt.%), the color of the powders quickly changed to slight yellow or orange when exposed to the ambient atmosphere. Higher loadings showed more intense colors already on the filter. Subsequent exposure (days) of the powders to ambient air induced further color change from yellow/orange to green/brown. The color change was reversible upon heat treatment resulting in almost white to orange powders under dehydrated conditions. This color change is attributed to a change of coordination from tetrahedral to a highly distorted VO_6 environment upon hydration [29]. This indicates that all samples exhibit highly dispersed and reactive VO_x surface species which react with the ambient moisture forming hydrated vanadia species [30–32].

3.2. Nitrogen adsorption

Nanosized catalyst particles with specific surface areas in the range of 119–333 $m^2\ g^{-1}$ (Table 1) were made by FSP. Only slight variation of the surface area (±10 $m^2\ g^{-1}$) was observed for three different charges of the same sample composition (10 V—Si, 20V—Si) underscoring the good reproducibility of the FSP synthesis. An increase in surface area was noticed for catalysts with low (1–10 wt.%) V_2O_5 contents. After passing the maximum (333 $m^2\ g^{-1}$) at 10 wt.%, the surface area steadily decreased reaching a value (119 $m^2\ g^{-1}$) for 50 wt.% V_2O_5/SiO_2 significantly lower than for pure FSP-made SiO_2 (292 $m^2\ g^{-1}$). This is attributed to the presence of separate V_2O_5 crystals with significant larger particle size which reduces the overall surface area. A similar trend with an SSA maximum at low dopant content (around 5–10 wt.%) was observed already previously for FSP-made Ta_2O_5/SiO_2 [33], $Cs_2O/Pt/Al_2O_3$ [22], and ZnO-containing SiO_2 [34]. In these studies [22,33], it was shown by means of NH_3 TPD experiments that the particle surface is indeed enriched with the doping metal-oxide and significantly different from pure FSP-made silica [33] or alumina [22], respectively. Therefore, the increase in SSA with increasing vanadia content up to 10 wt.% V_2O_5 could be related to a possible influence of the vanadium constituent on the SiO_2 sintering rate. Probably the presence of highly dispersed V atoms on the silica surface reduces particle sintering rate which results in smaller primary particles and therefore higher SSA. Rossetti et al. [11] also found a maximum in SSA even though particles were formed by a different formation mechanism. The highest SSA was measured for 28 wt.% V_2O_5, and generally the catalysts had significantly lower surface areas (<80 $m^2\ g^{-1}$) at similar composition compared to the FSP-made catalysts reported here. For a flame-based process with relative low precursor concentration (0.2 M), low surface areas in the range of 14 (pure SiO_2) to 80 $m^2\ g^{-1}$ (28 wt.% V_2O_5) were achieved by using tetraethoxysilane (TEOS) as Si precursor. In other studies, specific surface areas for flame-made SiO_2 were in the range of 300 $m^2\ g^{-1}$ for both vapor-fed diffusion flame [19] and liquid-fed flame spray pyrolysis [33] using TEOS as Si precursor. This difference can mainly be attributed to the use of low enthalpy (1400–1530 kJ mol^{-1}) solvents (ethanol and propionic acid) for the precursors and the very low pressure drop (0.4 bar) over the dispersion nozzle used by Rossetti et al. [11]. The low enthalpy density in the precursor and the reduced enthalpy of the pilot flame igniting the spray facilitate the droplet-to-particle formation route instead of complete combustion of the precursor and particle nucleation from the gas phase [23] which usually results in a more homogeneous particle size distribution with small primary particles [27]. Additionally the low pressure drop of the O_2 dispersion gas, resulting in subsonic gas flow at the nozzle tip, induced a poor dispersion of the liquid favoring inhomogeneous particle formation and low SSA powders [21,35].

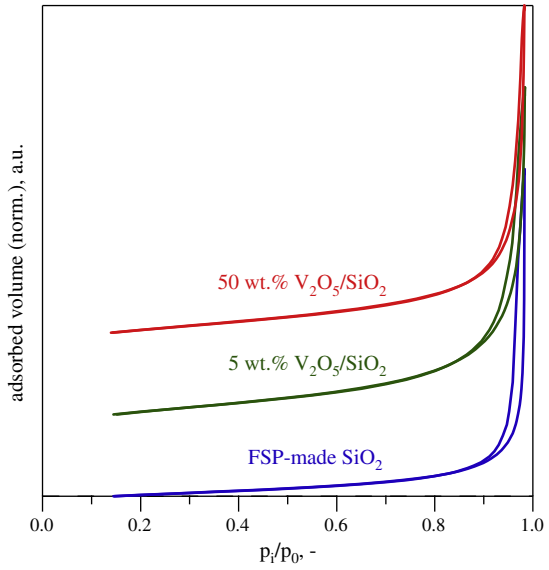

Fig. 1. Nitrogen adsorption–desorption isotherms of pure FSP-made SiO_2, and the 5V—Si and 50V—Si catalysts.

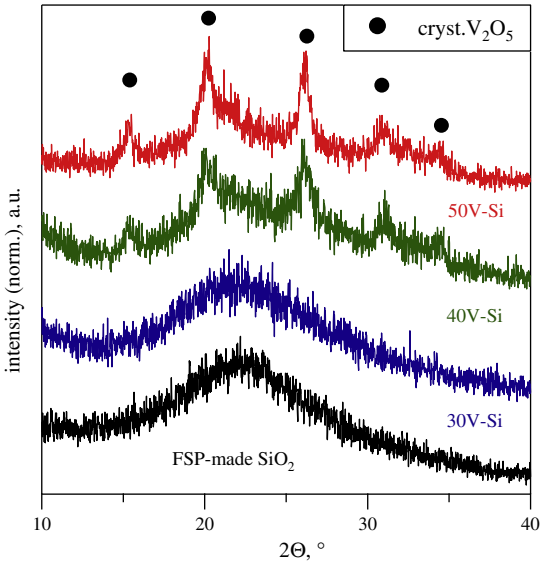

Fig. 2. XRD pattern of flame-made V_2O_5/SiO_2 samples containing 0–50 wt.% V_2O_5. Circles indicate the peaks of crystalline V_2O_5.

Nitrogen adsorption–desorption isotherms of the pure SiO_2, 5V—Si, and 50V—Si are shown in Fig. 1 as representative examples. They reveal the typical hysteresis characteristics of non-porous flame-made materials independent of the vanadia loading and catalyst particle size [26,36]. Clearly, the increase of the SSA at low vanadia contents (Table 1) is not related to any porosity of the catalyst particles but to the decrease in SiO_2 primary particle size during the particle formation process (coagulation and sintering) by addition of V_2O_5. This corroborates the already discussed gas-to-particle formation route of the catalysts presented here. Note that in the materials prepared with the flame conditions used by Rossetti et al., up to 44% (pure SiO_2) and 33% (10 wt. V_2O_5/SiO_2) of the measured BET surface area was attributed to the presence of micropores [11].

3.3. X-ray diffraction

XRD for the as-prepared V_2O_5/SiO_2 catalyst (Fig. 2) revealed the typical hump observed for amorphous flame-made silica and no indications of V_2O_5 crystals or solid solutions up to a vanadia loading as high as 30 wt.% (9.5 V nm^{-2}). This stands in contrast to flame-made V_2O_5/SiO_2 [11], which showed already at 28 wt.% vanadia loading crystalline V_2O_5 domains in the XRD, and corroborates different particle formation routes in the flame which can be explained by different process conditions. The use of high enthalpy solvents and high dispersion of the liquid induce particle nucleation from the gas phase favoring first the nucleation of SiO_2 because of the high boiling point temperature compared to V_2O_5. Therefore, VO_x condensation on the already formed silica surface is expected that will result in an enrichment of V at the support surface rather than forming a solid solution, as already observed for flame-made TiO_2 supported V_2O_5 catalysts before [13,19]. Additionally, the big difference in ionic radii of V^{5+} (54 Å) and Si^{4+} (40 Å) makes an incorporation of V atoms into the amorphous tetrahedral SiO_2 structure or even substitution of Si atoms very unlikely. To the best of our knowledge, no reports exist on vanadia/silica catalysts stating the formation of a solid solution of vanadium in the silica matrix. On the other hand, several studies report the formation of solid solutions with either TiO_2, ZrO_2, or CeO_2 but not with SiO_2 for V_2O_5/TiO_2—SiO_2 [37], V_2O_5/ZrO_2—SiO_2 [38], and V_2O_5/Ce_xZr—SiO_2 [39] systems, respectively. Therefore, the formation of a solid solution seemed rather unlikely. At higher V loadings (>30 wt.% V_2O_5), clear reflections arising from crystalline V_2O_5 (circles, Fig. 2) were detected around 2Θ = 14.5°, 20.3°, 26.1°, 30.9°, and 34.3°, indicating the formation of separate vanadia crystals at such high loadings (>9.5 V nm^2) and reducing the overall SSA (Table 1). A similar trend was observed for Ta_2O_5/SiO_2 particles made by flame spray pyrolysis at 45 wt.% of Ta_2O_5 [33].

3.4. TEM

The sample containing 10 wt.% V_2O_5 (Fig. 3a) showed the typical non-porous, highly aggregated, and fractal structure of flame-made SiO_2-based mixed oxides [33]. The EDX halo (Fig. 3a inset) clearly indicates the presence of only amorphous material as no diffraction pattern is visible. At higher loadings (50 wt.% V_2O_5, Fig. 3b), clear crystal planes are discernible, indicating the presence of crystalline domains and therefore corroborating the results of XRD (Fig. 2) which verified the presence of V_2O_5 crystals at these high vanadia loadings. Interlattice distances were found to be ca. 6.5 Å and therefore resemble the (0 1 0) crystal plane of pure V_2O_5, indicating that the crystal is not distorted by Ti atoms in interstitial positions. These crystalline domains were surrounded or could possibly even be covered by amorphous silica. Due to the higher vanadium content in the precursor solution, nucleation and particle formation of vanadia could happen earlier in the flame and thereby allowing the silica to cover the V_2O_5 in the sintering step. Similar morphology of segregated crystal domains at high dopant contents has been observed before for FSP-made Ta_2O_5/SiO_2 [33] and TiO_2/SiO_2 made in diffusion flame [40].

3.5. Temperature-programmed reduction

TCD signals measured during TPR of the 3–50 wt.% V_2O_5/SiO_2 and pure flame-made V_2O_5 are shown in Fig. 4. At very low V-coverage (0.6–1.0 V nm^{-2}, up to 5 wt.%), the reduction peak was broad and became sharper for higher V_2O_5 contents. The maximum reduction peak temperature (T_{max}, Table 1) for catalysts of 3–20 wt.% vanadia content was rather constant in the range of 587–596 °C, indicating an almost comparable reducibility of the VO_x species present in this range of vanadia loading. Increasing the V_2O_5 content to 25 wt.% increased the T_{max} to 609 °C and a distinct

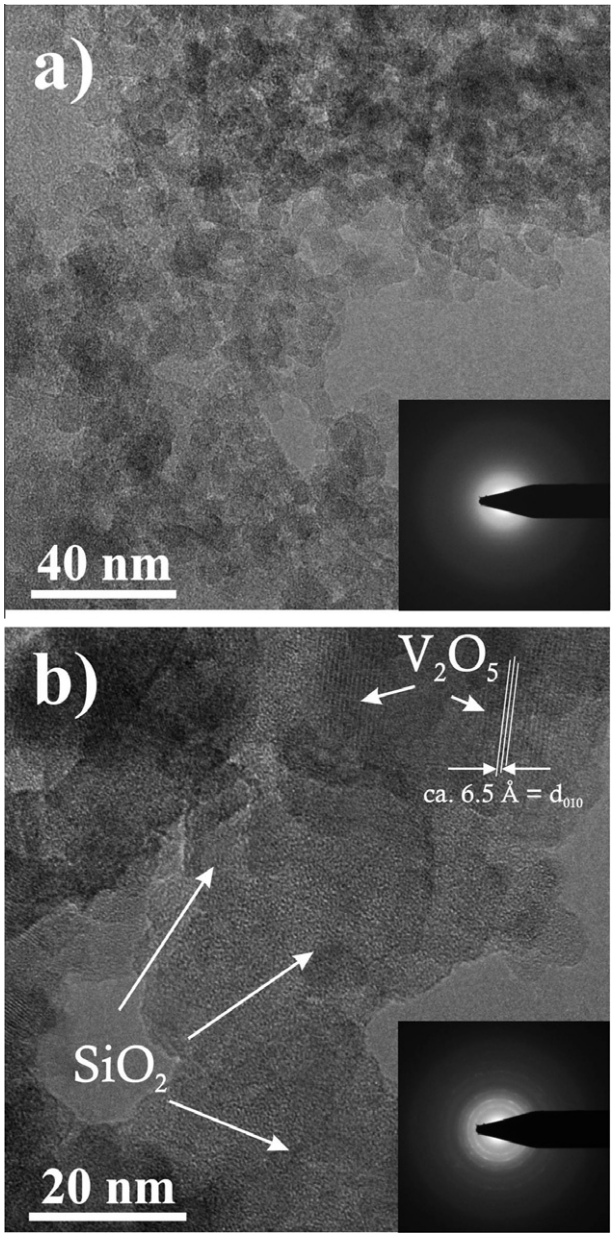

Fig. 3. TEM images of the 10 wt.% (a) and 50 wt.% (b) V_2O_5/SiO_2 samples. Only amorphous particles are detected for the 10V—Si catalysts while the 50V—Si sample clearly shows the presence of crystalline domains (EDX inset) which can be attributed to crystalline V_2O_5 with lattice fringes of ca. 6.5 Å.

shoulder appeared in the reduction profile. Clear assignment of VO_x species based on the maximum reduction peak and comparison to literature is rather difficult as the peak position can substantially be influenced by the experimental conditions applied [41,42]. All measurements were taken with a constant amount of reducible species (V) to exclude a shift due to the measurement parameters and not to the different structure of VO_x species [42]. Therefore we consider any significant shift to higher reduction temperatures at increasing vanadia loadings as indicative of a structural difference in the VO_x surface species. The relative stable peak temperature for the catalysts $\leqslant$20 wt.% V_2O_5 is indicative of a rather similar V dispersion in all these samples. Due to the absence of any other reduction peak at lower temperature, the observed peak temperatures likely indicate dominantly isolated tetrahedral VO_x species although they appeared at higher temperature than for wet-chemistry derived materials [14,18,43]. The shift in T_{max} (Table 1, Fig. 4)

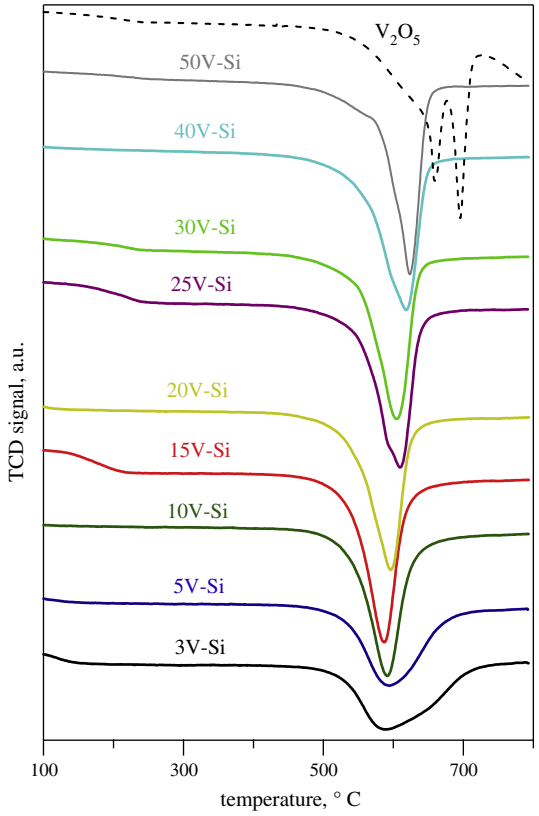

Fig. 4. TPR profiles of flame-made V_2O_5/SiO_2 with vanadia loadings ranging from 3 to 50 wt.% and the reduction profile of pure flame-made V_2O_5. Conditions: 10 mL min^{-1} 5 vol.% H_2 in Ar; heating rate 10 °C min^{-1}.

at higher loadings could be attributed to the presence of crystalline V_2O_5 domains. For sol–gel prepared particles of comparable composition and V surface density, a similar behavior of the shift in the reduction peak temperature was reported and was attributed to the presence of V_2O_5 domains [18]. Additionally, the shoulder visible in the reduction profile of the >25 wt.% V_2O_5 catalysts can be interpreted as a sign of stepwise reduction of different VO_x species [44], indicating different reducibility of the corresponding species, as already observed for FSP-made V_2O_5/TiO_2 [13,26].

The average oxidation state (AOS) after reduction (Table 1) decreased from 3.8 at low ($\leqslant$1 V nm^{-2}) to 3.6 at higher V surface density ($\geqslant$2 V nm^{-2}), indicating a slightly stronger reduction of the VO_x species present at high loadings. Comparable results were observed for the AOS of sol–gel made and impregnated catalysts [14,18].

Due to the presence of catalytically less favorable crystalline V_2O_5 in samples containing >30 wt.%, as confirmed by XRD (Fig. 2) and TEM (Fig. 3), the following characterization was focused on the catalysts containing 3–25 wt.% vanadia. These catalysts were considered to be the most interesting for the catalytic tests.

3.6. Raman spectroscopy

For characterization of the VO_x species, Raman spectroscopy was performed under dehydrated conditions for the flame-made V_2O_5/SiO_2 catalysts. For high V contents (>25 wt.% V_2O_5, not shown), dominantly crystalline V_2O_5 even for the XRD amorphous as-prepared 30V—Si catalysts was detected. In Fig. 5, the Raman spectra of the low V surface density (0.6 V nm^{-1}) calcined (400–600 °C) and dehydrated 3V—Si catalyst are shown. Dehydration

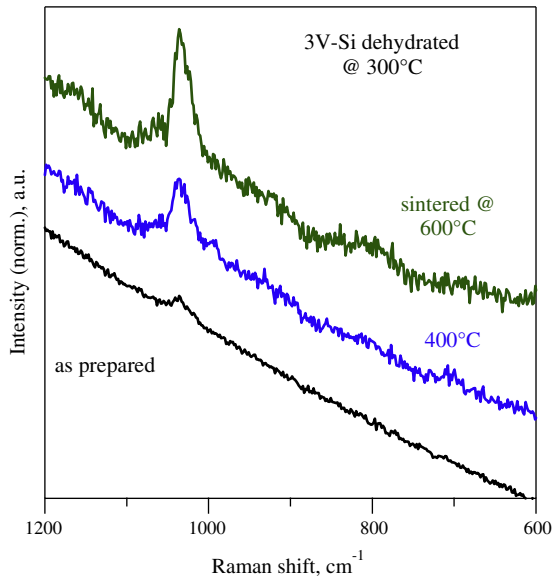

Fig. 5. Raman spectra of dehydrated 3V—Si catalyst: in as-prepared state and after calcination at 400 and 600 °C. Only Raman bands assigned to monomeric VO_x species were detected. Spectra were recorded at room temperature after calcination in air (5 °C min^{-1}, 5 h) and dehydration at 300 °C in synthetic air.

temperature was set to relative low temperature (300 °C) to avoid any alteration of the sample during dehydration. The spectra of the as-prepared catalyst showed a band at 1034 cm^{-1} which can be attributed to the symmetric stretching mode of V=O bonds indicating the presence of isolated monomeric VO_x species in tetrahedral coordination [45–47]. Upon calcination at 600 °C in air, the signal of the monomeric band became more prominent. This is probably related to the fact that dehydration temperatures for V_2O_5/SiO_2 need to be significantly higher than those of e.g. V_2O_5/TiO_2 for which temperatures up to 300 °C were sufficient for complete dehydration [13]. Flame-made SiO_2 is known to be hydrophilic with a high stability of chemisorbed OH groups even at high temperatures (>300 °C) [48]. Therefore, the additional heat treatment by calcination at 400 °C and higher caused a more effective dehydration of the sample resulting in higher intensity of the monomeric VO_x band. No additional bands, possibly indicating other VO_x species (oligomeric or crystalline), were detected corroborating our reduction peak assignment in the TPR analysis (Fig. 4). The heat treatment had only small influence on the surface area of this sample which dropped from 333 to around 320 m^2g^{-1}, corroborating the high stability of these flame-made V_2O_5/SiO_2 catalysts, not only in terms of VO_x species structure but also particle morphology.

Based on these findings, the dehydration temperature in the *in-situ* cell for the following Raman measurements was set to 500 °C to assure complete dehydration. In Fig. 6, representative spectra recorded at 500 °C over a period of 72 h are shown for selected V_2O_5/SiO_2 catalysts. It should be noted that a slight shift (≈5 cm^{-1}) of the detected bands to lower wave numbers was observed for the spectra recorded at 500 °C compared to those cooled down to room temperature after dehydration (not shown).

The 5V—Si (Fig. 6a) and 15V—Si (Fig. 6b) show the band located at 1034 cm^{-1} but no band at 993 cm^{-1}, indicating the absence of crystalline V_2O_5 [47] and corroborating the results of XRD analysis (Fig. 2). Even after 72 h at 500 °C, the structure of the VO_x species did not change, further supporting the excellent stability of monomeric VO_x species in flame-made V_2O_5/SiO_2. Note that the 15V—Si catalyst exhibited a V surface density of 3.3 V nm^{-2} which exceeds the "theoretical monolayer" coverage of classical wet-impregnated V_2O_5/SiO_2 systems. The classical catalyst systems show crystalline V_2O_5 at significantly lower V surface density: usually below 2.3 V nm^{-2} [4–7] or as low as 1.3 for zeolithe type materials [2,14]. Clearly, the presence of highly stable (up to 500 °C), exclusively amorphous monomeric VO_x species at such high loadings is a unique characteristic of FSP-made V_2O_5/SiO_2 catalysts.

The observed bands around 603 and 802 cm^{-1} originate from the SiO_2 support and were identified as Si—O—Si stretching modes [5,45]. The intensity of these bands constantly decreased with increasing V_2O_5 content of the catalysts, indicating the covering of these SiO_2 species by surface VO_x species. A broad band around 915 cm^{-1} was discernible for both the 5V—Si and 15V—Si catalysts, which was not observed for the 3V—Si catalysts (Fig. 5). This band is usually attributed to V—O—V vibrations [14,47] which would indicate the rather atypical presence of small amounts of oligomeric VO_x species on SiO_2 even at this low V surface density (1–3.3 V nm^{-2}). Recently, however, this assignment was challenged by several other EXAFS and Raman studies [7,49,50] (and references therein) attributing this band clearly to symmetric V—Si—O vibrations. Additionally, the shoulder at around 1060 cm^{-1}, visible for catalysts 3, 5, 10, and 15V—Si, is attributed to the corresponding asymmetric vibrations of these V—Si—O bands [7,49,50]. Therefore, bands around 915, 1034, and 1065 cm^{-1} in the flame-made V_2O_5/SiO_2 catalysts are assigned accordingly, and the presence of dominantly isolated monomeric VO_x species in tetrahedral coordination on the silica surface up to a V surface density of 3.3 V nm^{-2} and 500 °C is assumed. These observations further support the role of V species on altering the surface of SiO_2 and delaying its sintering especially at low vanadia contents.

Upon increasing the vanadia content to 20 wt.% (Fig. 6c), the bands at 993 and 695 cm^{-1} indicating crystalline V_2O_5 became apparent . Showing only a small peak after 1 h at 500 °C, the intensity of the bands progressively increased with time, indicating the transformation of amorphous VO_x species into crystalline domains under these conditions. Additionally, vanishing of the V—O—Si bands at 910 cm^{-1} at 24 h at 500 °C was observed, indicating a decrease of the fraction of V—O—Si bonds and corroborating the transformation of monomeric VO_x species into crystalline V_2O_5. The band of the monomeric VO_x species, however, was still dominant although Raman spectroscopy is more sensitive for crystalline metal oxides [51] corroborating a high amount of monomeric VO_x species and only trace amounts of crystalline V_2O_5 even at such high vanadia loading (4.6 V nm^{-2}). This is different for the 25V—Si catalysts shown in Fig. 6d. Here, the crystalline bands at 528, 695, and 998 cm^{-1} are dominant features. The increase in intensity of the 993 cm^{-1} band relative to the monomeric band at 1034 cm^{-1} with longer exposure time at high temperature indicates a change of the VO_x species structure on the particle surface, forming more and more crystalline V_2O_5. Nevertheless, a small peak at 1034 cm^{-1} is visible and suggests the presence of monomeric VO_x species even at high VO_x density (6.9 V nm^{-2}). It should be noted that spectra of hydrated samples for both the as-prepared 20V—Si and 25V—Si catalysts (not shown) did not show any bands related to crystalline V_2O_5 in agreement with the XRD results (Fig. 2). Therefore, it can be concluded that the crystalline V_2O_5 detected with Raman at 500 °C (Fig. 6c and d) was formed during dehydration treatment.

Fig. 7 depicts Raman spectra of the 10V—Si, 15V—Si, and 20V—Si catalysts dehydrated at 500 °C after their use in catalytic tests for >24 h on stream at 550 °C. Note that after exposure to reaction conditions, the 10V—Si showed only bands due to amorphous monomeric VO_x similar to the as-prepared state (not shown), whereas in 15V—Si and 20V—Si crystalline V_2O_5 prevailed. For latter compositions, clear structural changes in the VO_x species occurring under reaction conditions can be observed when compared to the as-prepared sample (Fig. 6b and c). Raman bands of the amor-

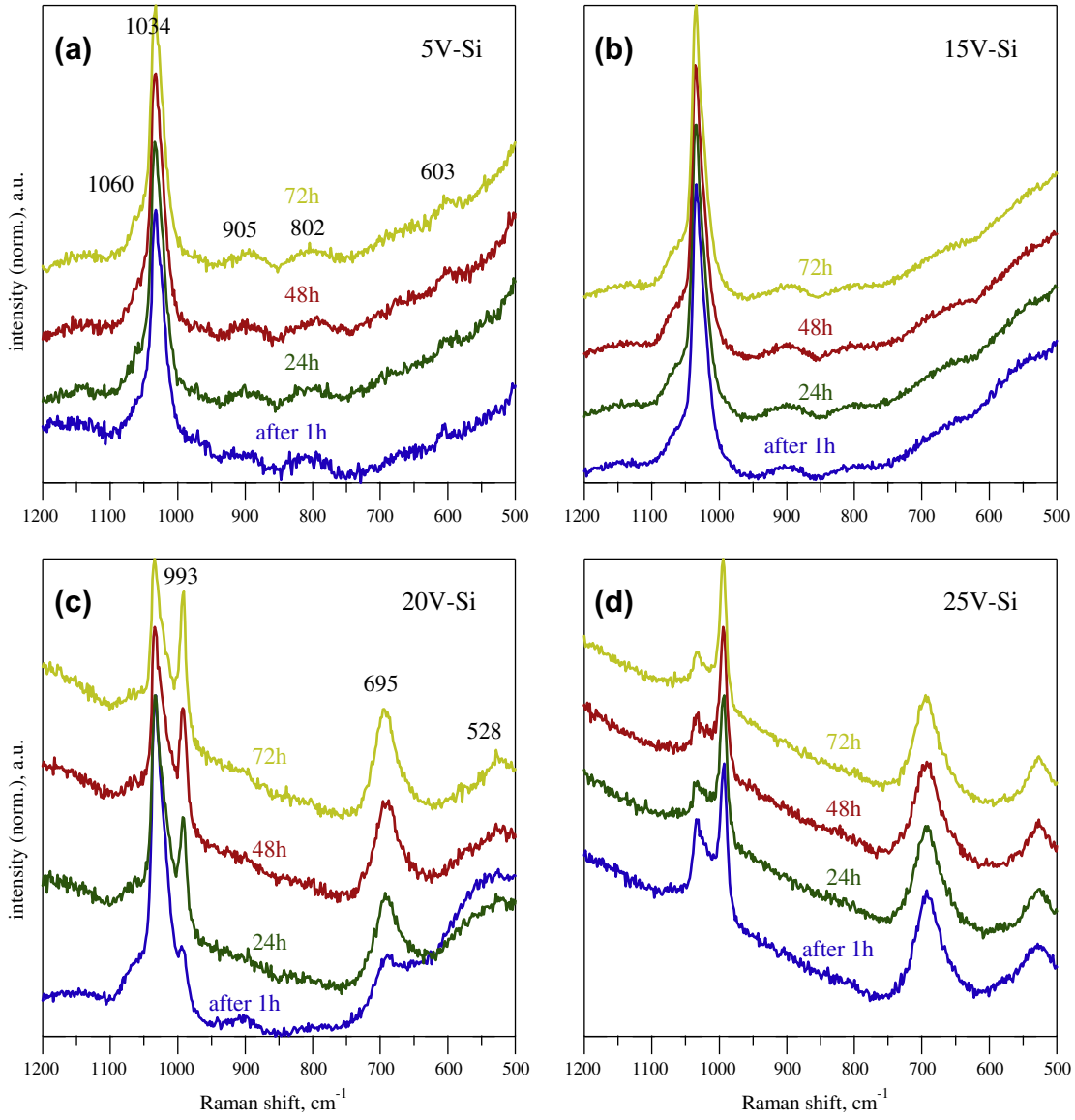

Fig. 6. Long-term *in-situ* Raman spectra recorded at 500 °C in synthetic air for 72 h for the 5V—Si (a), 15V—Si (b), 20V—Si (c), and 25V—Si (d) catalysts. Conditions see experimental part.

phous monomeric VO_x species are significantly lower in intensity, while the band at 998 cm^{-2} representing crystalline V_2O_5 increased in intensity, indicating a transition from amorphous to crystalline vanadia during reaction for these two catalysts. Nevertheless, a small peak at 1037 cm^{-1} can be observed for the 15V—Si catalyst corroborating still the presence of monomeric VO_x species even under reaction conditions, whereas for the 20V—Si catalyst the monomeric band is hardly visible and crystalline V_2O_5 seems to be dominating.

3.7. NMR analysis

Additional to Raman spectroscopy, selected catalysts were characterized by ^{51}V MAS NMR to gain more information about the structure of the VO_x species present at different V surface density. The chemical shift parameters of the catalysts under hydrated and dehydrated conditions are summarized in Table 2. In Fig. 8, the ^{51}V MAS NMR spectra under hydrated conditions of the 3V—Si and 25V—Si catalysts are presented. Both spectra show an isotropic chemical shift at around −580 ppm with the components of an anisotropic chemical shift tensor at −101, −427, and −1244 ppm, according to the simulation of ^{51}V MAS NMR spectra. An isotropic chemical shift in the range of −570 to 590 ppm was observed for other silica-supported vanadia catalysts [32,52] and V—silicalites [30] before. This peak resembles quite closely the environment of crystalline V_2O_5 but can clearly be assigned to V^{+5} five coordinated hydrated tetrahedral surface species [32,52]. A close inspection of the 25V—Si spectra reveals a slightly asymmetric peak width in the high field, indicating the presence of a second V species in this sample with an isotropic chemical shift around −610 ppm. This signal can be attributed to distorted octahedral environment of crystalline V_2O_5 [53] corroborating the results from Raman analysis (Fig. 6d). A distinct peak, however, was not detected which is likely due to the lower sensitivity of NMR for crystalline V_2O_5 compared to Raman [32] and the dominant peak of the hydrated tetrahedral VO_x species. Additionally, the absence of any peak feature of four coordinated tetrahedral VO_4 species in the range of −700 ppm in the hydrated state proofs the high dispersion, accessibility, and reactivity of the V surface sites in the flame-made V_2O_5/SiO_2 catalysts in contrast to sol–gel derived materials where inaccessible V

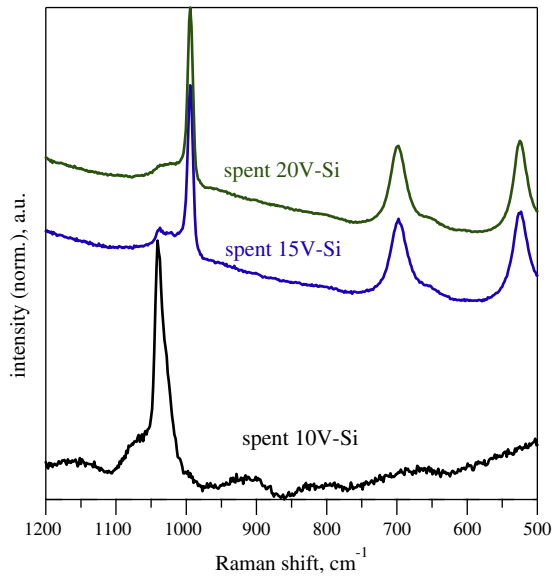

Fig. 7. Raman spectra of the spent 10V—Si, 15V—Si, and 20V—Si catalysts dehydrated at 500 °C. Only Raman bands assigned to amorphous VO_x species were detected for the 10 wt.%V_2O_5/SiO_2 catalysts, while dominantly crystalline V_2O_5 was detected in the catalyst containing 15 or 20 wt.%. vanadia after the catalytic tests.

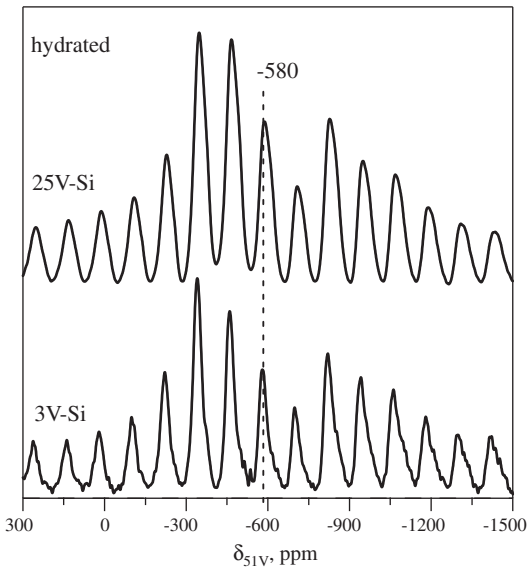

Fig. 8. ^{51}V MAS NMR spectra of the 3V—Si and 25V—Si catalysts under hydrated conditions. Conditions see experimental part.

Table 2
Chemical shift parameters of the flame-made V_2O_5/SiO_2 catalysts.

Sample	Isotropic chemical shift δ_{iso}[a] (ppm)	Anisotropic chemical shift tensor[b] (ppm)		
		δ_{11}	δ_{22}	δ_{33}
All hydrated	−580 ± 10	−101 ± 10	−427 ± 10	−1244 ± 10
3V—Si	−715 (V—O—Si)	−485	−507	−1155
10V—Si	−712 (V—O—Si)	−487	−509	−1139
20V—Si	−615 (V—O—V)	−125	−452	−1268
	−692 (V—O—Si)	−468	−489	−1120
25V—Si	−616 (V—O—V)	−127	−453	−1270
	−691 (V—O—Si)	−467	−489	−1119

[a] Values obtained from measured MAS NMR spectrum.
[b] Values obtained from simulated MAS NMR spectrum.

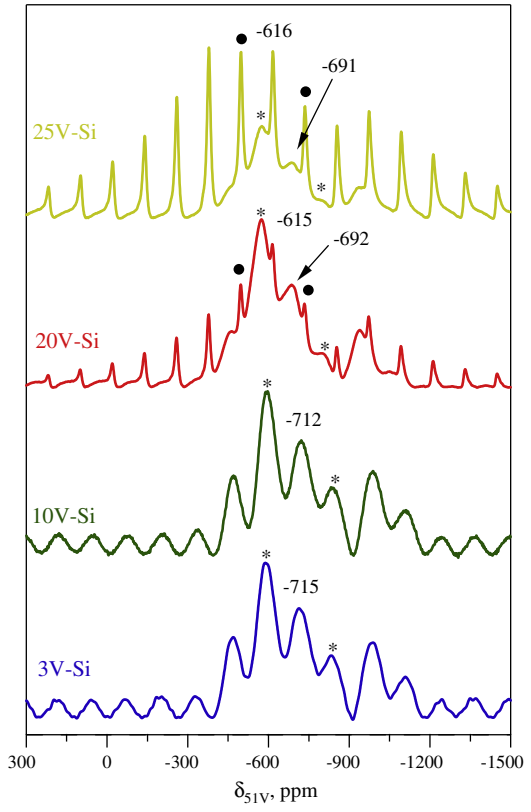

Fig. 9. ^{51}V MAS NMR spectra of the 3V—, 10V—, 20V—, and 25V—Si catalysts under dehydrated conditions. Symbols ● and * indicate the sidebands of the isotropic shifts at ca.−616 ppm (V—O—V) and −691, and 712 ppm (V—O—Si), respectively.

sites in tetrahedral coordination were found [30–32]. It should be noted that the V^{51} MAS NMR spectra under hydrated conditions of all V_2O_5/SiO_2 catalysts in a broad range of V surface densities (0.6–6.9 V nm^{-2}) were similar, and no significant difference could be observed. Additionally, all anisotropic chemical shift tensors are close to axial.

This, however, is completely different for the dehydrated case shown in Fig. 9 and Table 2. At low V surface density (<6.6 V nm^{-2}), the only isotropic shift is detected around −715 ppm. This peak shift upon dehydration was observed for various V_2O_5/SiO_2 made by different synthesis methods before and clearly shows the presence of isolated four coordinated dehydrated V^{+5} species with V=O and three V—O—Si bonds to the support [30,52]. This data supports the assignments of the 915 cm^{-1} (and 1060 cm^{-1}) shift in the Raman spectra (Fig. 6) to the V—O—Si bridging bonds rather than to oligomeric V—O—V species which were not detected by NMR. The spectra of the 15V—Si catalysts (not shown) were similar to the one obtained for the 10V—Si sample which corroborates the results from Raman and TPR analysis and confirms the high V dispersion for the as-prepared V_2O_5/SiO_2 catalysts made by FSP. The NMR spectrum of the 20V—Si catalyst instead shows a narrow peak at −615 ppm in the dehydrated state. This peak indicates the presence of V—O—V bonds of crystalline V_2O_5 [53,54] in agreement with Raman analysis (Fig. 6c). Additionally, comparable to the low V surface density catalysts a clear peak at −692 ppm was detected and attributed, though slightly shifted to higher chemical shifts, to the presence of distorted tetrahedral surface V sites. Despite the high V surface density of 4.6 V nm^{-2}, a significant amount of monomeric VO_x species seemed to be present on the catalyst surface, corroborating the Raman results shown in Fig. 6c. Further

increase of the vanadia loading (25V—Si) resulted in an enhanced intensity of the −616 ppm peak compared to the −691 ppm peak, indicating the presence of dominantly crystalline V_2O_5 and lower fraction of monomeric species compared to the 20V—Si, as already observed in the Raman analysis (Fig. 6d).

3.8. Catalytic performance

The activity of selected V_2O_5/SiO_2 catalysts was tested under steady-state conditions at 400–550 °C with a constant gas hourly space velocity (GHSV, 45,000 L kg_{cat}^{-1} h^{-1}) and propane/oxygen/nitrogen ratio (1:1:3). In Fig. 10, the C_3H_8 conversion (X_{C3H8}) is plotted as a function of the reaction temperature. Pure FSP-made SiO_2 (filled circles) showed only minor catalytic activity while doping the silica with V resulted in an increase of the conversion of propane. Therefore, catalytic activity and conversion of the flame-made V_2O_5/SiO_2 catalysts strongly depended on the V surface density and increased with temperature. Increasing the vanadia content from 3 (0.6 V nm^{-2}, 3V—Si) to 20 wt.% (4.6 V nm^{-2}, 20V—Si) caused a 4–5 times higher propane conversion at given reaction temperature. The significant increase in conversion with V loading can be attributed to the presence of a high concentration of isolated tetrahedral VO_x species completely accessible to the reactants on the catalyst surface. Interestingly, this increase seems to be only little dependent on the structure of the VO_x species. Catalysts containing >10 wt.% V_2O_5 showed the presence of crystalline V_2O_5 (Figs. 6c, 7 and 9) which apparently had no detrimental effect on the activity. This is in contrast to V-SBA-15 [14] or impregnated mesocellulous silica foams (MCF) [2], where already the appearance of crystalline VO_x species caused a decrease in propane conversion at a surface density of around 1.2–1.6 V nm^{-2}. This corroborates the extremely high dispersion of VO_x species of FSP-made V_2O_5/SiO_2 catalysts even at high V surface density, making these catalysts very attractive for the oxidative dehydrogenation of propane.

Only when the vanadia loading was increased further (6.9 V nm^{-2}, 25V—Si) and crystalline V_2O_5 became the dominating VO_x species (Fig. 6d), for which a considerable amount of vanadium is not accessible to the reactants, a lower propane conversion (Fig. 10) was observed. This is illustrated in more detail in Fig. 11

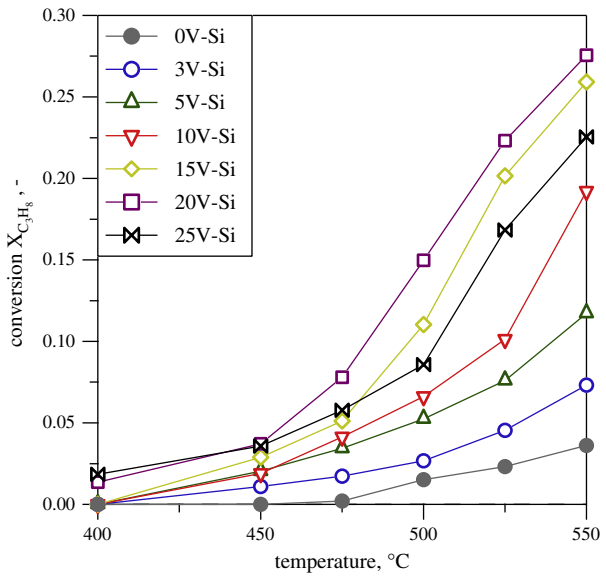

Fig. 10. Propane conversion for all tested V_2O_5/SiO_2 catalysts with variation of reaction temperature. Reaction conditions: m_{cat} = 0.2 g, GHSV = 45,000 L g_{cat}^{-1} h^{-1}, C_3H_8:O_2:N_2 = 1:1:3.

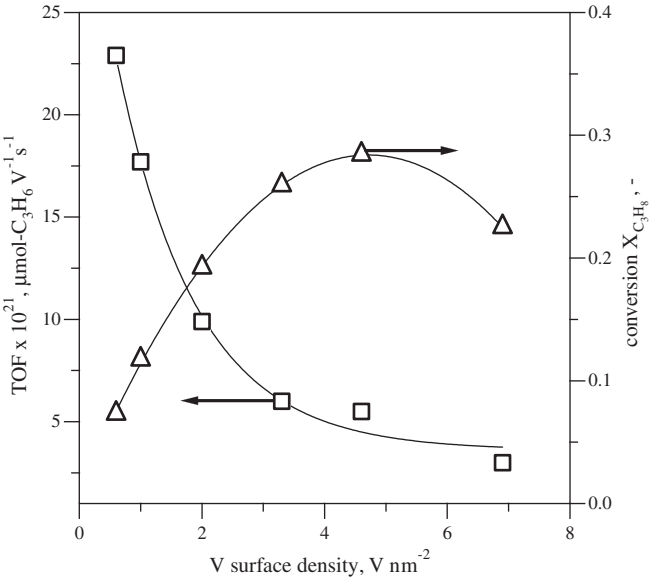

Fig. 11. Variation of the turn-over-frequencies (TOF, cubes) and propane conversion (X_{C3H8}, triangles) with the V surface densities. Reaction conditions: m_{cat} = 0.2 g, GHSV = 45,000 L g_{cat}^{-1} h^{-1}, $T_{reaction}$ = 550 °C, C_3H_8:O_2:N_2 = 1:1:3.

which compares the turnover frequency (TOF, squares) and propane conversion (triangles) at constant reaction temperature (550 °C) and GHSV (45,000 L kg_{cat}^{-1} h^{-1}) as function of the V surface density. A clear conversion maximum around 4.6 V nm^{-2} (20 wt.% V_2O_5) could be observed, indicating that not all vanadia was accessible (active) beyond this loading due to an increased fraction of crystalline vanadia (Figs. 6 and 8). The TOF of propene production strongly decreased with increasing vanadia loading. The decrease followed an almost exponential decay with a strong decrease up to 2 V nm^{-2} (10 wt.% V_2O_5) (close to the "theoretical monolayer") and reached an almost asymptotic value for catalysts with >3 V nm^{-2}. A similar trend at low V surface density was observed for vanadia-based MCF [2] and SBA-15 [14] catalysts. The latter, however, showed a drop in TOF over one order of magnitude when increasing the V surface density from 0.2 to 2.4 V nm^{-2}, suggesting a low dispersion in these catalysts, and corroborating the high accessibility of VO_x species in flame-made V_2O_5/SiO_2. The most active VO_x species of flame-made V_2O_5/SiO_2 seems to be the isolated tetrahedral sites, dominantly present in the low V surface density ($\leqslant$2 V nm^{-2}) catalysts in agreement with other studies [2,14,16–18].

Not only activity, also selectivity to the corresponding light olefins is of high importance for ODH catalysts. Usually, selectivity to propene is strongly related to conversion. When looking at the selectivity with increasing reaction temperature, the following was observed: The two low V surface density flame-made V_2O_5/SiO_2 catalysts (3V—Si and 5V—Si) with a high fraction of isolated VO_x species showed a rather constant selectivity of around 55% and 45%, respectively, independent of the reaction temperature and conversion change. A similar trend was observed for 10V—Si (2 V nm^{-2}) up to a reaction temperature of 525 °C before a drop (40–32%) in propene selectivity occurred. This contrasts the behavior of conventional mesoporous [17] and flame pyrolyzed [11] V_2O_5/SiO_2 catalysts which showed a strong dependency of the propene selectivity on the reaction temperature at comparable vanadia V surface density or vanadia loading, respectively. For higher vanadia contents (15–25 wt.%), all catalysts showed a steadily decreasing selectivity with increasing reaction temperature.

The influence of the conversion on the selectivity is additionally illustrated in Fig. 12a. Low V surface density catalysts 3V—Si and

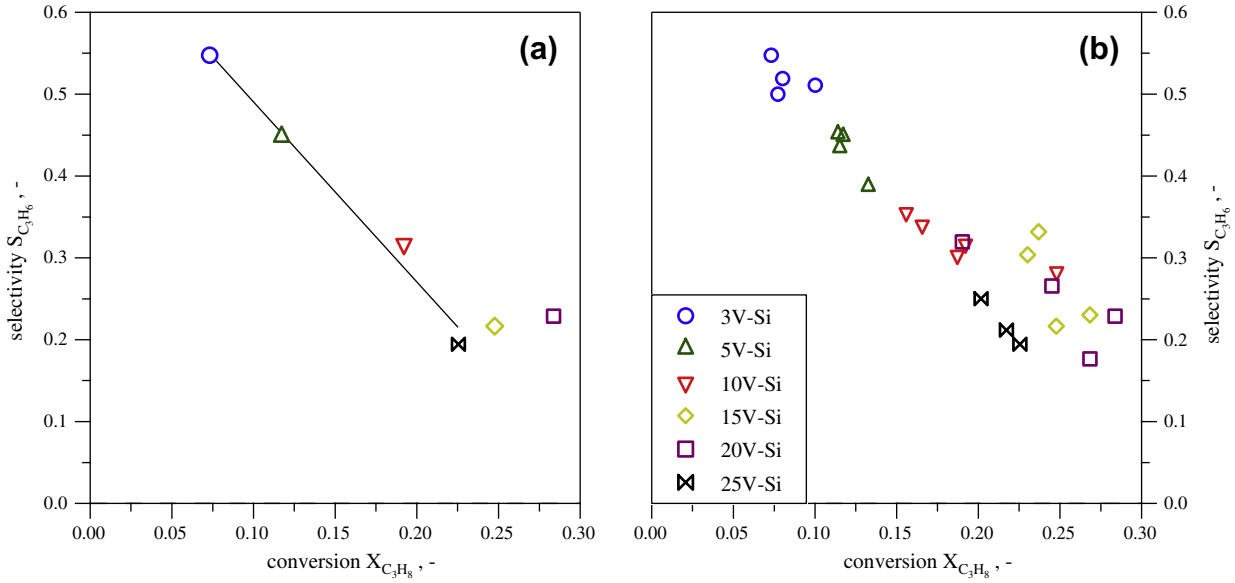

Fig. 12. Propene selectivity as function of propane conversion on flame-made V_2O_5/SiO_2 catalysts for (a) constant GHSV (45,000 L g_{cat}^{-1} h^{-1}) and (b) with variation of GHSV (37,500–60,000 L g_{cat}^{-1} h^{-1}). Reaction conditions: m_{cat} = 0.2 g, $T_{reaction}$ = 550 °C, C_3H_8:O_2:N_2 = 1:1:3.

5V—Si, showing the lowest propane conversion, afforded the highest propene selectivities. With increasing the V loading and thus activity, propene selectivity decreased even for catalysts containing exclusively isolated VO_x species (3V—, 5V— and 10V—Si) corroborating that these species are probably active for both the dehydrogenation step and the further oxidation of propene to CO_x depending on the distances of the active sites [15]. Focusing on the 3, 5, 10, and 25V—Si catalysts, an almost linear decrease of the propene selectivity with increasing conversion could be observed. Starting from 55% at 7% conversion (3V—Si), the propene selectivity decreased to 20% for a conversion of 22.5% (25V—Si). Clearly, the catalysts 15V—Si and 20V—Si showed significant difference in this dependency with higher conversions (>25%) but similar or increasing propene selectivity up to 28% (20V—Si). This behavior may be related to the observed structural rearrangement of the amorphous VO_x species into V_2O_5 crystallites upon heating to temperatures $\geqslant$500 °C during the catalytic tests (Figs. 6c and 7) while retaining a considerable fraction of monomeric VO_x species.

In order to investigate the dependency of the propene selectivity on the propane conversion in more detail, a different set of experiments with variation of the GHSV (from 37,500 to 60,000 L kg_{cat}^{-1} h^{-1}) were performed. In Table 3, the product distribution for the shortest contact time, which resulted in the highest propene yield for the tested catalysts, is shown. It can be noticed that flame-made V_2O_5/SiO_2 resulted in the formation of an appreciable amount of acrolein almost independent of the vanadia loading. Similar catalytic behavior has been reported for vanadia-based catalysts on mesoporous silica SBA-15 [14]. In the latter study, however, only catalysts with low vanadia loading (<1 V nm^{-1}) exhibiting almost exclusively isolated tetrahedral VO_x species showed the formation of oxygenated products. This could be considered as indication for the high VO_x dispersion with a significant amount of monomeric species of FSP-made V_2O_5/SiO_2 even at high vanadia loadings. It is notable that with increasing vanadia content, the ratio of CO_2/CO decreased (Table 3). This tendency was valid for the whole range of propane conversion investigated. Apparently, the increase in V surface density and the presence of crystalline VO_x species in flame-made V_2O_5/SiO_2 favor the formation of CO rather than CO_2 at high conversion as has been observed for other flame-made V_2O_5/SiO_2 catalysts before [11].

As can be seen in Fig. 12b, the selectivity vs. conversion with variation of the contact time followed the same trend as observed in Fig 12a: increasing propane conversion leads to lower propene selectivity. Only minor influence, however, was observed for both the low V surface density catalysts 3V—Si and 5V—Si. For higher vanadia loadings (>10 wt.% V_2O_5), the propane conversion and propene selectivity changed significantly with variation of the GHSV. While the 10V—Si and 25V—Si catalysts showed an almost linear dependency of the propene selectivity, again the catalysts 15V—Si and 20V—Si showed a considerable deviation from this behavior as discussed earlier. Apparently, the presence of

Table 3
Conversion and selectivity of the flame-made V_2O_5/SiO_2 catalysts in the oxidative dehydrogenation of propane at 550 °C.[a]

Sample	C_3H_8 conv. (%)	Selectivity (%)					Ratio CO_2/CO	TOF × 10^{21} (μmol C_2H_6 V^{-1} s^{-1})	STY_{C3H6}[b] (kg $kg_{cat}^{-1}h^{-1}$)
		C_3H_6	C_2H_4	C_3H_4	CO_2	CO			
0V—Si	3.7	40.4	2.2	–	36.0	5.9	6.1	–	0.3
3V—Si	8.5	50.0	2	2.4	34.6	9.2	3.8	29.3	0.9
5V—Si	11.5	43.4	1.7	3.0	29.0	12.2	2.4	22.5	1.1
10V—Si	16.6	34.0	1.2	3.3	25.6	23.5	1.1	12.2	1.2
15V—Si	23.7	33.2	1.0	4.3	26.4	22.3	1.2	11.7	1.8
20V—Si	19	31.2	1.3	4.3	21.9	25.4	0.9	6.9	1.4
25V—Si	20.2	25.0	0.7	3.2	24.1	32.1	0.8	4.6	1.1

[a] Reaction conditions: m_{cat} = 0.2 g, GHSV = 60,000 L $kg_{cat}^{-1}h^{-1}$, C_3H_8:O_2:N_2 = 1:1:3.
[b] Rate of formation of propene per unit mass of catalyst per time, STY_{C3H6} (space–time yield).

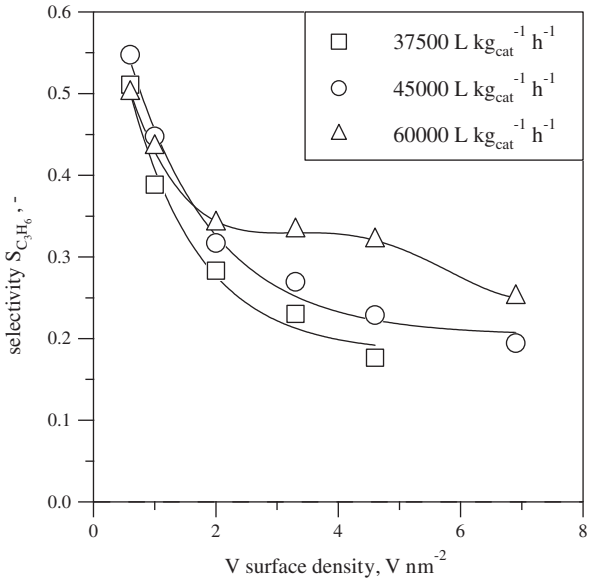

Fig. 13. Propene selectivity as function of V surface density and GHSV of flame-made V_2O_5/SiO_2 catalysts. Reaction conditions: m_{cat} = 0.2 g, $T_{reaction}$ = 550 °C, C_3H_8:O_2:N_2 = 1:1:3. Propene selectivity at 10% conversion (b) as function of *V* surface density.

some small crystalline V_2O_5 domains had virtually no influence on the propene selectivity. Additionally to the observed conversion dependency, Fig. 12 indicates that the selectivity depends also on the vanadia loading. This is illustrated in Fig. 13 in more detail. Low V surface density catalysts (3V—Si and 5V—Si) show the higher propene selectivity almost independent of the GHSV (Fig. 13a). Increasing the vanadia loading reduced the propene selectivity to around 20% for the catalyst with the highest V surface density and crystalline V_2O_5 present. At intermediate V surface densities (10–20 wt.% V_2O_5), however, a clear dependency of the propene selectivity on the GHSV could be observed. Shorter contact times resulted in only a minor decrease (3% for the 15V—Si and 7% for the 20V—Si) in propane conversion but a significant increase in propene selectivity by 10% and 14% (absolute) for the 15V—Si and 20V—Si catalysts, respectively. Although these catalysts contained a significant amount of crystalline V_2O_5 (Figs. 6c and 7), they showed the best catalytic performance as indicated by the highest space–time yield ($STY_{C_3H_6}$ in kg kg_{cat}^{-1} h^{-1}, Table 3) of all tested flame-made V_2O_5/SiO_2 catalysts. The STY was always close to or above 1 which is significantly higher than that of impregnated V catalysts supported on mesoporous MCM-41 [18], but lower than those on MCF supported catalysts [2]. For an industrially interesting application of such catalysts, the STY should be at least 1 kg propene per kg_{cat}^{-1} h^{-1} [55], corroborating further the possible potential of such flame-made V_2O_5/SiO_2 catalysts in an industrial process.

4. Conclusions

We applied one-step flame spray pyrolysis as a fast and highly reproducible synthesis method for non-porous nanosized V_2O_5/SiO_2 catalyst for the oxidative dehydrogenation of propane. The BET surface area of as-prepared catalysts depended on the V_2O_5 content, resulting in up to 330 m^2 g^{-1} for catalysts with <3.3 V nm^{-1} V surface density (<15 wt.% V_2O_5). Such flame-made catalysts showed unique properties in terms of V dispersion exhibiting dominantly isolated tetrahedral coordinated VO_x species up to a relative high V surface density of 3.3 V nm^{-2}, as confirmed by Raman and NMR analysis. This is to the best of our knowledge the highest V surface density reported for exclusively isolated VO_x species on any SiO_2 support so far. The VO_x species were highly stable up to 500 °C as determined by *in-situ* Raman spectroscopy. Higher contents (up to 30 wt.% V_2O_5) resulted in the presence of small V_2O_5 crystallites not detectable by XRD, and no indications of inaccessible V sites in the silica bulk framework were found. Further increase of the vanadia loading caused formation of separate V_2O_5 particles in the flame, as detected by XRD and evidenced by TEM. FSP-made V_2O_5/SiO_2 catalysts showed a similar reducibility for vanadia loadings of 3–15 wt.% V_2O_5 with reduction peak temperature around 590 °C, while higher contents needed higher temperatures for reduction.

The catalytic activity strongly depended on the amount of vanadia on the SiO_2 surface and increased with reaction temperature and V_2O_5 loading despite the presence of crystalline V_2O_5 domains at relative high V surface density (3.3–4.6 V nm^{-2}). Low V surface density (<3.3 V nm^{-2}) catalysts showed very stable and high propene selectivity (40–55%) at intermediate propane conversion, while higher contents resulted in higher conversion but lower propene selectivity. Catalysts exhibiting V surface densities higher than 2 V nm^{-2} showed structural rearrangement of the present VO_x species during the catalytic tests, forming an increased amount of crystalline V_2O_5 domains. Despite the presence of the latter, the highest propene yield was measured for the catalyst containing 15 wt.% V_2O_5 or 3.3 V nm^{-2}. Based on the presented results, the most promising catalysts under conditions applied should have an intermediate to high V surface density around 3 V nm^{-2}. Best performance is expected at short contact times (GHSV > 50,000) and moderate to high reaction temperatures (500–550 °C). The reasonably high space–time yield achieved (1.8) indicates the potential of such flame-made catalysts for the oxidative dehydrogenation of propane. Further optimization of the ODH with these flame-derived V_2O_5/SiO_2 catalysts seems feasible.

Acknowledgments

We thank Tobias Vassella for experimental assistance and Dr. Frank Krumeich and the EMEZ (ETHZ) for TEM analysis. Financial support by ETH Research Grant TH-41 06-1 is gratefully acknowledged.

References

[1] F. Cavani, N. Ballarini, A. Cericola, Catal. Today 127 (2007) 113–131.
[2] Y.M. Liu, W.L. Feng, T.C. Li, H.Y. He, W.L. Dai, W. Huang, Y. Cao, K.N. Fan, J. Catal. 239 (2006) 125–136.
[3] G. Hammer, T. Lübcke, R. Kettner, M.R. Pillarella, H. Rechnagel, A. Commichau, H. Neumann, and B. Paczynska-Lahme, *Natural Gas*, in: Ullamann's Encyclopedia of Industrial Chemistry, Wiley-VCH Verlag GmbH & Co. KGaA, Weinheim, 2006.
[4] B. Grzybowska-Swierkosz, Appl. Catal. A – Gen. 157 (1997) 263–310.
[5] I.E. Wachs, B.M. Weckhuysen, Appl. Catal. A – Gen. 157 (1997) 67–90.
[6] A. Khodakov, B. Olthof, A.T. Bell, E. Iglesia, J. Catal. 181 (1999) 205–216.
[7] D.E. Keller, T. Visser, F. Soulimani, D.C. Koningsberger, B.M. Weckhuysen, Vib. Spectrosc. 43 (2007) 140–151.
[8] A.A. Lemonidou, L. Nalbandian, I.A. Vasalos, Catal. Today 61 (2000) 333–341.
[9] F. Arena, F. Frusteri, A. Parmaliana, Appl. Catal. A – Gen. 176 (1999) 189–199.
[10] H.J. Tian, E.I. Ross, I.E. Wachs, J. Phys. Chem. B 110 (2006) 9593–9600.
[11] I. Rossetti, L. Fabbrini, N. Ballarini, C. Oliva, F. Cavani, A. Cericola, B. Bonelli, M. Piumetti, E. Garrone, H. Dyrbeck, E.A. Blekkan, L. Forni, J. Catal. 256 (2008) 45–61.
[12] J. Keranen, P. Carniti, A. Gervasini, E. Iiskola, A. Auroux, L. Niinisto, Catal. Today 91-92 (2004) 67–71.
[13] B. Schimmoeller, H. Schulz, A. Ritter, A. Reitzmann, B. Kraushaar-Czarnetzki, A. Baiker, S.E. Pratsinis, J. Catal. 256 (2008) 74–83.
[14] Y.M. Liu, Y. Cao, N. Yi, W.L. Feng, W.L. Dai, S.R. Yan, H.Y. He, K.N. Fan, J. Catal. 224 (2004) 417–428.
[15] T. Blasco, J.M.L. Nieto, Appl. Catal. A – Gen. 157 (1997) 117–142.
[16] Y.M. Liu, Y. Cao, S.R. Yan, W.L. Dai, K.N. Fan, Catal. Lett. 88 (2003) 61–67.

[17] J. Santamaria-Gonzalez, J. Luque-Zambrana, J. Merida-Robles, P. Maireles-Torres, E. Rodriguez-Castellon, A. Jimenez-Lopez, Catal. Lett. 68 (2000) 67–73.
[18] B. Solsona, T. Blasco, J.M.L. Nieto, M.L. Pena, F. Rey, A. Vidal-Moya, J. Catal. 203 (2001) 443–452.
[19] W.J. Stark, K. Wegner, S.E. Pratsinis, A. Baiker, J. Catal. 197 (2001) 182–191.
[20] H. Poelman, B.F. Sels, M. Olea, K. Eufinger, J.S. Paul, B. Moens, I. Sack, V. Balcaen, F. Bertinchamps, E.M. Gaigneaux, P.A. Jacobs, G.B. Marin, D. Poelman, R. De Gryse, J. Catal. 245 (2007) 156–172.
[21] L. Mädler, H.K. Kammler, R. Mueller, S.E. Pratsinis, J. Aerosol. Sci. 33 (2002) 369–389.
[22] B. Schimmoeller, F. Hoxha, T. Mallat, F. Krumeich, S.E. Pratsinis, A. Baiker, Appl. Catal. A – Gen. 374 (2010) 48–57.
[23] R. Strobel, A. Baiker, S.E. Pratsinis, Adv. Powder Technol. 17 (2006) 457–480.
[24] H. Schulz, L. Madler, R. Strobel, R. Jossen, S.E. Pratsinis, T. Johannessen, J. Mater. Res. 20 (2005) 2568–2577.
[25] W.J. Stark, S.E. Pratsinis, A. Baiker, J. Catal. 203 (2001) 516–524.
[26] B. Schimmoeller, H. Schulz, S.E. Pratsinis, A. Bareiss, A. Reitzmann, B. Kraushaar-Czarnetzki, J. Catal. 243 (2006) 82–92.
[27] R. Jossen, S.E. Pratsinis, W.J. Stark, L. Madler, J. Am. Ceram. Soc. 88 (2005) 1388–1393.
[28] R. Strobel, S.E. Pratsinis, J. Mater. Chem. 17 (2007) 4743–4756.
[29] X.T. Gao, S.R. Bare, B.M. Weckhuysen, I.E. Wachs, J. Phys. Chem. B 102 (1998) 10842–10852.
[30] G. Centi, S. Perathoner, F. Trifiro, A. Aboukais, C.F. Aissi, M. Guelton, J. Phys. Chem. 96 (1992) 2617–2629.
[31] A.E. Stiegman, H. Eckert, G. Plett, S.S. Kim, M. Anderson, A. Yavrouian, Chem. Mater. 5 (1993) 1591–1594.
[32] C.B. Wang, G. Deo, I.E. Wachs, J. Catal. 178 (1998) 640–648.
[33] H. Schulz, L. Madler, S.E. Pratsinis, P. Burtscher, N. Moszner, Adv. Funct. Mater. 15 (2005) 830–837.
[34] T. Tani, L. Madler, S.E. Pratsinis, J. Mater. Sci. 37 (2002) 4627–4632.
[35] G.L. Chiarello, I. Rossetti, L. Forni, J. Catal. 236 (2005) 251–261.
[36] R. Strobel, W.J. Stark, L. Madler, S.E. Pratsinis, A. Baiker, J. Catal. 213 (2003) 296–304.
[37] G.C. Bond, S.F. Tahir, Appl. Catal. 71 (1991) 1–31.
[38] B.M. Reddy, B. Chowdhury, I. Ganesh, E.P. Reddy, T.C. Rojas, A. Fernandez, J. Phys. Chem. B 102 (1998) 10176–10182.
[39] B.M. Reddy, P. Lakshmanan, P. Loridant, Y. Yamada, T. Kobayashi, C. Lopez-Cartes, T.C. Rojas, A. Fernandez, J. Phys. Chem. B 110 (2006) 9140–9147.
[40] A. Teleki, S.E. Pratsinis, K. Wegner, R. Jossen, F. Krumeich, J. Mater. Res. 20 (2005) 1336–1347.
[41] G.C. Bond (Ed.), Catal. Today 20 (1994) 1–184.
[42] D.A.M. Monti, A. Baiker, J. Catal. 83 (1983) 323–335.
[43] M.M. Koranne, J.G. Goodwin, G. Marcelin, J. Catal. 148 (1994) 369–377.
[44] Y.H. Kim, H.I. Lee, Bull. Korean Chem. Soc. 20 (1999) 1457–1463.
[45] X.T. Gao, S.R. Bare, J.L.G. Fierro, M.A. Banares, I.E. Wachs, J. Phys. Chem. B 102 (1998) 5653–5666.
[46] M. Schraml-Marth, A. Wokaun, and A. Baiker, in: 6th Working Conf on Applied Surface Analysis: Secondary Neutral Mass Spectrometry and Laser Photoionization, Proceedings, 1990, pp. 87–91.
[47] G.T. Went, S.T. Oyama, A.T. Bell, J. Phys. Chem. 94 (1990) 4240–4246.
[48] R. Mueller, H.K. Kammler, K. Wegner, S.E. Pratsinis, Langmuir 19 (2003) 160–165.
[49] N. Magg, B. Immaraporn, J.B. Giorgi, T. Schroeder, M. Baumer, J. Dobler, Z.L. Wu, E. Kondratenko, M. Cherian, M. Baerns, P.C. Stair, J. Sauer, H.J. Freund, J. Catal. 226 (2004) 88–100.
[50] Z.L. Wu, S. Dai, S.H. Overbury, J. Phys. Chem. C 114 (2010) 412–422.
[51] S.S. Chan, I.E. Wachs, L.L. Murrell, J. Catal. 90 (1984) 150–155.
[52] N. Das, H. Eckert, H.C. Hu, I.E. Wachs, J.F. Walzer, F.J. Feher, J. Phys. Chem. 97 (1993) 8240–8243.
[53] O.B. Lapina, V.M. Mastikhin, A.V. Nosov, T. Beutel, H. Knozinger, Catal. Lett. 13 (1992) 203–211.
[54] O.B. Lapina, V.M. Mastikhin, A.A. Shubin, V.N. Krasilnikov, K.I. Zamaraev, Prog. Nucl. Magn. Reson. Spectrosc. 24 (1992) 457–525.
[55] J.B. Stelzer, J. Caro, M. Fait, Catal. Commun. 6 (2005) 1–5.